Asymmetric triplex metallohelices with high and selective activity against cancer cells

Alan D. Faulkner,[a,†] Rebecca A. Kaner,[a,†] Qasem M. A. Abdallah,[b] Guy Clarkson,[a] David J. Fox,[a] Pratik Gurnani,[a] Suzanne E. Howson,[a] Roger M. Phillips,[c] David I. Roper,[d] Daniel H. Simpson,[a,d] Peter Scott,[a,*]

[a] Department of Chemistry, University of Warwick, Gibbet Hill Road, Coventry, CV4 7AL, UK

[b] College of Pharmacy, Taif University, PO Box 888, 21974 Taif, Saudi Arabia

[c] Institute of Cancer Therapeutics, University of Bradford, Bradford, BD7 1DP, UK

[d] School of Life Sciences, Gibbet Hill Campus, University of Warwick, Coventry, CV4 7AL, UK

* Author to whom correspondence and requests for materials should be addressed. Email address: peter.scott@warwick.ac.uk

† These authors contributed equally to this work

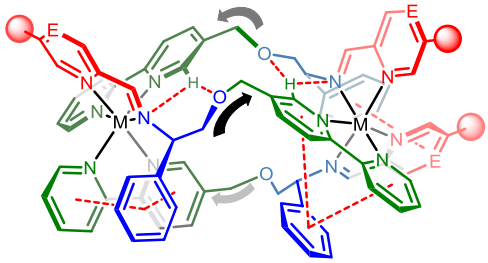

An antiparallel strand arrangement in water-soluble helicates creates an amphipathic functional topology akin to that of host-defence peptides. High and selective cancer cell line toxicity is exhibited, causing dramatic changes in the cell cycle without DNA damage, and remarkably there is no significant toxicity to *MRSA* and *E. coli*.

Abstract

Small cationic amphiphilic α-helical peptides are emerging as agents for the treatment of cancer and infection, but they are costly and display unfavourable pharmacokinetics. Helical coordination complexes may offer a three-dimensional scaffold for the synthesis of mimetic architectures; however, the high symmetry and modest functionality of current systems offer little scope to tailor the structure to interact with specific biolomolecular targets, or to create libraries for phenotypic screens. Here we report the highly stereoselective asymmetric self-assembly of very stable, functionalised metallohelices. Their anti-parallel Head-to-Head-to-Tail 'triplex' strand arrangement creates an amphipathic functional topology akin to that of the active sub-units of *e.g.* host-defence peptides and p53. The metallohelices display high, structure-dependent toxicity to the human colon carcinoma cell-line HCT116 $p53^{++}$ causing dramatic changes in the cell cycle without DNA damage. They have lower toxicity to human breast adenocarcinoma cells (MDA-MB-468), and most remarkably they show no significant toxicity to the bacteria *MRSA* and *E. coli*.

150 words

The active regions of many disease-resisting proteins – such as the human antimicrobial host-defence peptide cathelicidin LL-37[1] and p53[2] which prevents mutations in the genome – are based around a cationic amphipathic α-helix. Correspondingly, these small units have been investigated as clinical antibiotic and anticancer compounds.[3-6] Significant progress has also been made in the development of synthetic derivatives with greater structural integrity, such as stapled peptides, [7,8] and peptidic foldamers based on unnatural building blocks.[9-11] In addition, several non-peptide synthetic scaffolds have been put forward[12,13] in an effort to provide synthetically tractable systems while still presenting key recognition features of the α-helix.

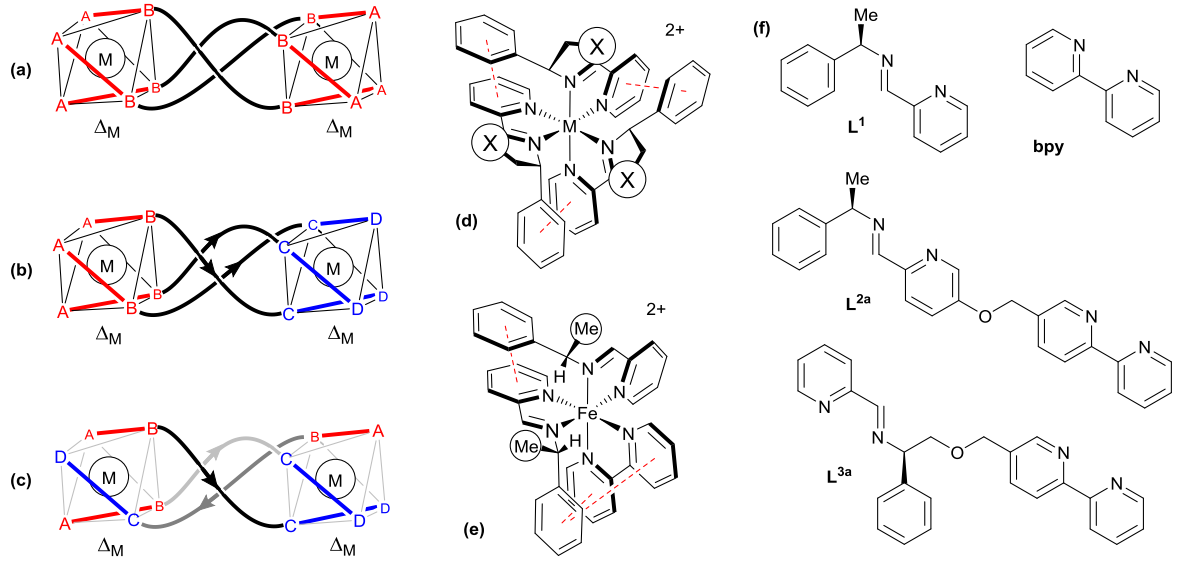

Fig 1 | Metallohelix architectures. Metal helicates are usually based on rigid ditopic bidentate ligands **AB**–**BA** giving – at octahedral centres – D_3-symmetric enantiomers [M_2(**AB**–**BA**)$_3$] **(a)**, while the use of directional ligands **AB**–**CD** leads to mixtures of C_3-symmetric Head-to-Head-to-Head **(b)** and C_1-symmetric Head-to-Head-to-Tail "triplex" architectures **(c)**. A highly stereoselective approach to this latter architecture has now been designed and realised. Computational investigations showed that π-stacking phenomena in stereogenic units of type **(d)** based on **L**^{1} were modulated by introducing **bpy** units as in **(e)**. A series of **L**^{1}–**bpy** (i.e. **AB**–**CD**) ditopic ligands such as **L**^{2a} and **L**^{3a} **(f)** were subsequently used to make a library of triplex metallohelices.

Certain self-assembling multimetallic coordination complexes, known as helicates[14] [Fig 1(a)], resemble α-helices in terms of their diameter and charge, but since they are synthesised using symmetric rigid ligands **AB**–**BA** they have much higher symmetry. When *directional* ligands **AB**–**CD** are employed, Head-to-Head-to-Head [HHH, Fig. 1(b)] and Head-to-Head-to-Tail [HHT, (c)] constitutions are introduced, and a total of four pairs of enantiomers [M_2(**AB**–**CD**)$_3$] are possible. Correspondingly, these architectures are observed in mixtures of stereo- and/or optical isomers.[15-22] Also, most helicates contain little if any external functionality, are incompatible with water, and are not readily available in enantiomerically pure form.[23] For example, a prototypical [M_2(**AB**–**BA**)$_3$] system[24] for which several biological studies have been reported[25-27] is based on few analogues, requires chromatographic resolution or lengthy syntheses, and undergoes significant hydrolysis on

experimental timescales (*vide infra*). Thus, although helicates are appealing as a potential framework for peptidomimetic chemistry, they cannot currently provide us with anything approaching the exquisite functionality and topography present in natural α-helix systems.

Recently we showed that by linking two diastereomerically pure tris-chelate metal complex units[28-31] via the groups X [Fig 1(d)] we could access water-compatible, stereochemically inert, functionalised helices we called flexicates.[32,33] These compounds are highly symmetrical, with the general structure of Fig1(a). We previously established that the very high stereoselection (Δ *v*. Λ) in the monometallics arises largely from steric effects, while the arene π-interactions shown are principally responsible for *fac*/*mer* selectivity and the unusual stability of flexicates in water.[28] Since the *mer* configurations cannot be present in a helicate-like structure in any event we reasoned that π-stacking effects might be exploited to deliver stereoselection for the desirable, asymmetric HHT isomers of $[M_2(\mathbf{AB}–\mathbf{CD})_3]$ while still retaining control over helicity. Here we report a highly stereoselective self-assembly of diverse, stable, functionalised, metallohelices with anti-parallel 'triplex' arrangement of strands. These metallohelices have amphipathic topology and very high, structure-dependent, selective biological activity. As such we believe that these triplex metallohelices represent a new and versatile α-helix mimetic structure type.

Results

Design, synthesis and characterisation

We considered a directional ditopic ligand design **AB**–**CD** where **AB**– is provided by a derivative of $\mathbf{L}^1$ [Fig 1], and –**CD** comes from an achiral bidentate; here we chose 2,2'-bipyridine (bpy) because it is expected to form strong intramolecular π-stacks with co-ligands $\mathbf{L}^1$ *but not with itself*, and also since a large number of derivatives are known. The feasibility of a diastereoselective HHT isomer synthesis using putative new helicands such as $\mathbf{L}^{2a}$ and $\mathbf{L}^{3a}$ was assessed first by computing the relative energies of individual metal units expected in that architecture (Table 1, entries 1-4).

For $[Fe\mathbf{L}^1{}_2(bpy)]^{2+}$ six isomers are possible, but only the Δ- and Λ-*cis*,*cis* diastereomers have the appropriate connectivity to be present in the HHT structure. Of these, the Δ diastereomer [depicted in Fig 1(e)] was found to be the more stable by 9.62 kcal mol^{-1} due to a strong steric clash involving methyl groups in the Λ isomers. Additionally, both isomers feature one parallel-offset π-stacking interaction[34] between a metal-coordinated pyridine ring and the neighbouring $\mathbf{L}^1$ ligand, and a second interaction between $\mathbf{L}^1$ and bpy. Grimme has noted that the magnitude of such interactions increases with the number of rings involved.[35]

For the doubly bpy-substituted unit $[Fe\mathbf{L}^{1}(bpy)_2]^{2+}$ the two possible isomers are C_1 symmetric diastereomers. Both contain a parallel-offset π-stacking interaction between the phenyl ring and an adjacent bpy ligand, but sterics again dictate that the Δ enantiomer is the lower in energy, this time by 2.58 kcal mol^{-1} (entry 4). We conclude that the presence of one or two $\mathbf{L}^{1}$-type ligands is sufficient to deliver stereocontrol at a single metal centre, and thus that a HHT structure [Fig 1(c)] in this series is likely to be homochiral, *i.e*. have the same absolute configuration at both metal centres.

Entry	Complex	isomer	Relative energy kcal mol^{-1}	Population/% (298 K)
1	*cis*,*cis*,S_C-$[Fe\mathbf{L}^{1}_2(bpy)]^{2+}$	S_C,Δ_{Fe}	0.0	-
2		S_C,Λ_{Fe}	+9.62	-
3	S_C-$[Fe\mathbf{L}^{1}(bpy)_2]^{2+}$	S_C,Δ_{Fe}	0.0	-
4		S_C,Λ_{Fe}	+2.58	-
5	$[Zn_2\mathbf{L}^{2a}{}_3]$	$S_C,\Delta_\alpha,\Delta_\beta$,HHT	0.00	93.8
6		$S_C,\Delta_\alpha,\Delta_\beta$,HHH	+0.95	6.2
7		$S_C,\Delta_\alpha,\Lambda_\beta$,HHT	+4.66	0.0
8		$S_C,\Delta_\alpha,\Lambda_\beta$,HHH	+6.48	0.0
9	$[Fe_2\mathbf{L}^{2a}{}_3]$	$S_C,\Delta_\alpha,\Delta_\beta$,HHT	0.00	97.4
10		$S_C,\Delta_\alpha,\Delta_\beta$,HHH	+1.51	2.6
11		$S_C,\Delta_\alpha,\Lambda_\beta$,HHH	+7.62	0.00
12		$S_C,\Delta_\alpha,\Lambda_\beta$,HHT	+8.82	0.00
13	$[Zn_2\mathbf{L}^{3a}{}_3]$	$R_C,\Delta_\alpha,\Delta_\beta$,HHT	0.00	99.8
14		$R_C,\Delta_\alpha,\Delta_\beta$,HHH	+3.05	0.2
15		$R_C,\Delta_\alpha,\Lambda_\beta$,HHH	+4.11	0.0
16		$R_C,\Lambda_\alpha,\Lambda_\beta$,HHT	+10.39	0.0
17	$[Fe_2\mathbf{L}^{3a}{}_3]$	$R_C,\Delta_\alpha,\Delta_\beta$,HHT	0.00	99.5
18		$R_C,\Delta_\alpha,\Delta_\beta$,HHH	+2.50	0.5
19		$R_C,\Delta_\alpha,\Lambda_\beta$,HHH	+12.55	0.0
20		$R_C,\Delta_\alpha,\Lambda_\beta$,HHT	+17.64	0.0

Table 1 | Calculated energies (DFT) of selected isomers for monometallic units and metallohelices. In the stereochemical descriptors, subscripts α and β refer to the pyridineimine-rich and bpy-rich metal centres respectively. The equilibrium selectivities were determined the statistically corrected energies of each isomer at 298 K.

The potential effects of helication and the thermodynamic selectivity HHT *vs* HHH were then investigated for both Zn(II) and Fe(II) with $\mathbf{L}^{2a}$ and $\mathbf{L}^{3a}$: ligands for which reasonable synthetic routes were envisaged and a large number of derivatives are possible (*vide infra*). For the particular carbon-centred configurations used here, the homochiral (Δ,Δ) HHT isomers were found to be the lowest energy by between 0.95 and 3.05 Kcal mol^{-1} (Table 1, entries 5, 9, 13, 17), followed by the corresponding HHH. The effect of helication is also apparent; the homochiral HHH isomers are more stable than the corresponding mesocate-like structures (entry 6 v 8 etc). Following a correction for the fact that each HHT structure can be formed in three ligand permutations compared with only one for

each HHH, the estimated equilibrium selectivities for the asymmetric helicate are excellent, particularly for $\mathbf{L}^{3}$.

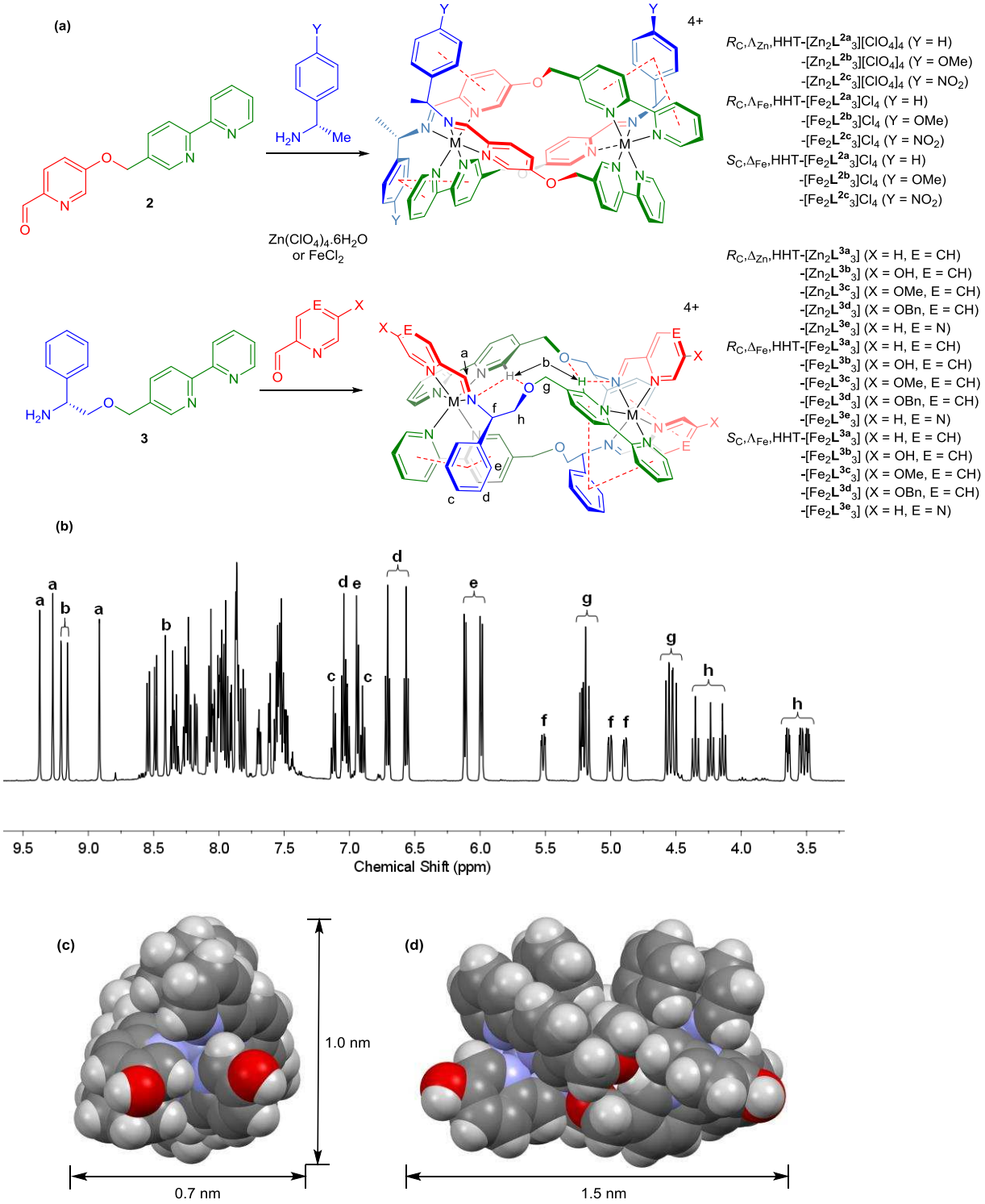

Fig 2 | Synthesis and characterisation of triplex metallohelices. (a) Self-assembly from versatile components of a wide range of functionalised helices in which the strands are arranged head-head-tail; (b) ^{1}H NMR spectrum and key assignments for R_C,Δ_{Zn},HHT-$[Zn_2\mathbf{L}^{3a}{}_3][ClO_4]_4$. The small singlet at 8.76 ppm may be due to the three spectroscopically equivalent imine protons in the C_3-symmetric HHH isomer. On this assumption the diastereomeric purity is >98%; (c) space-filling model of the cationic unit in R_C,Δ_{Zn},HHT-

$[Zn_2\mathbf{L}^{\mathbf{3b}}{}_3][ClO_4]_4$ from X-ray crystallography viewed along the Zn-Zn axis, showing the somewhat flattened architecture, and (d) rotated left by 90°. The three OH groups surround the basal plane while the upper ridge is comprised of π-stacked arenes.

The new compounds **2** and **3** were combined with a selection of metal sources, plus aldehydes or phenethylamines as shown in Fig 2 in one-pot reactions to give the two ranges of homochiral helicates shown. By analogy with the bi-directional motif of triplex DNA, we refer to these as *triplex* metallohelices. The compounds were characterised by NMR spectroscopy, mass spectrometry, UV/vis, circular dichroism, IR, thermogravimetry and microanalysis. For example, mixing three equivalents each of amine *R*-**3** and 2-pyridinecarboxaldehyde with two equivalents of $Zn(ClO_4)_2 \cdot 6H_2O$ led to the clean formation of R_C,Δ_{Zn},HHT-$[Zn_2\mathbf{L}^{\mathbf{3a}}{}_3][ClO_4]_4$. The ^{1}H NMR spectrum of this complex [Fig 1(b)] indicates the presence of three spectrocopically unique ligand environments. Of particular interest is that two of the bpy atoms $H^{\mathbf{b}}$ are observed at unusually low field (*ca* 9.2 ppm). We propose that this results from the close proximity (*ca* 2.5 Å) of these protons to the ether oxygen atom of an adjacent ligand as observed in the computed structure and as indicated in Figure 1(a). No such interaction is observed for the remaining H^b, the resonance being observed further up field at 8.41 ppm. Similarly, two sets of phenyl ring protons H^d and H^e (6.65-5.85 ppm) experience strong through-space shielding from the bpy unit of an adjacent ligand. These observations indicate that the solution structure corresponds very closely to that computed above. Overall, the equilibrium selectivity for the isomer shown is exceptionally good (>98%) and consistent with calculation (99.8% Table 1).

In the case of R_C,Δ_{Zn},HHT-$[Zn_2\mathbf{L}^{\mathbf{3b}}{}_3][ClO_4]_4$ very small needle like crystals were obtained by slow vapour diffusion of ethyl acetate into a solution of the compound in acetonitrile/methanol. An X-ray diffraction study confirmed the homochiral (Δ_{Zn}) HHT structure depicted in Figure 2(a), (c) and (d). The single "conventional" phenyl/pyridine π-stack has a centroid–centroid distance of *ca* 3.60 Å, within the range we have reported previously.[28] The two π-stacks between phenyl and 2,2'-bipyridine rings may be described by two such centroid-centroid distances: a shorter at 3.60-3.69 Å and a longer of 4.41-4.60 Å. The rings are close to parallel (*ca* 5˚) with interplanar distances of *ca* 3.38 Å, significantly shorter than those computed by Grimme for similar scenarios (*ca* 3.5 Å).[35] This may be due to the greatly increased polarity caused by coordination of the biaryl to the metal. The two cross-strand bpy-H→O interactions noted above are also observed (*ca* 2.5 Å). For the overall structure, and unlike conventional helicate systems, the triplex assembly leads to a slightly flattened structure [Fig 2(b),(c)] and pronounced asymmetry of functional group placement; a basal region contains the three hydroxyl groups and the structure narrows to a hydrophobic ridge comprising five π-stacked rings.

Water soluble triplex metallohelices were obtained using the above self-assembly reactions and iron(II) chloride. ^{1}H-NMR spectra were broadened in comparison with the Zn(II) systems but

well resolved and fully assigned ^{13}C spectra were obtained. Microanalysis, thermogravimetric analysis and mass spectra were also consistent with the proposed formulation. The CD spectra of the enantiomers in water were equal and opposite (see ESI), and the compounds were found to be remarkably stable. At pH 7 and 20 °C, no significant hydrolysis was detected over weeks for R_C,Λ_{Fe},HHT-[$Fe_2\mathbf{L^{2a}}_3$]Cl_4 and R_C,Λ_{Fe},HHT-[$Fe_2\mathbf{L^{3a}}_3$]Cl_4, compared to Hannon's cylinder[36] [$Fe_2(C_{25}H_{20}N_4)_3$]Cl_4 which in our hands decomposed far more rapidly. In strong acid (pH 1) the hydrolysis kinetics are cleanly first order and R_C,Λ_{Fe},HHT-[$Fe_2\mathbf{L^{2a}}_3$]Cl_4 was recorded to have $t_{1/2}$ of *ca* 10.3 h, compared to 1.4 h for [$Fe_2(C_{25}H_{20}N_4)_3$]Cl_4. Remarkably R_C,Λ_{Fe},HHT-[$Fe_2\mathbf{L^{3a}}_3$]Cl_4 is so stable to hydrolysis even at pH 1 that a half-life could not be recorded over 10 d. Furthermore, the compounds have excellent stability in the phosphate-rich RPMI-1640 cell growth medium over 96 h; for the same $\mathbf{L^{2a}}$ and $\mathbf{L^{3a}}$ compounds, 30% and 0% decay were observed, whereas [$Fe_2(C_{25}H_{20}N_4)_3$]Cl_4 decomposed by *ca* 90%.

Anticancer activity and mechanistic studies

The sixteen new water-soluble Fe(II) triplex systems were screened, along with cisplatin for comparison, for their activity against cancer cell lines MDA-MB-468 (human breast adenocarcinoma) and HCT116 $p53^{++}$ (human colon carcinoma with wild type p53). The latter was chosen following a recent report that FK-16 – a short amphipathic α-helix derived from the human host-defence peptide LL-37 – induced apoptosis in a closely related cell-line.[37] The resulting range of IC_{50} values indicated great selectivity, covering *ca* two orders of magnitude (0.5 – 70 μM) [Figs 3(a), (b)]. Notably, and in agreement with the stability studies above, no decolouration of the drug solutions was detected during the 96 h experiments.

In MDA-MB-468 the $\mathbf{L^2}$ compounds have moderate toxicity and do not display enantiomeric selectivity; the nitroarene enantiomers ($\mathbf{L^{2c}}$) alone had similar activity to cisplatin. In contrast, all Δ_{Fe}-$\mathbf{L^3}$ compounds are more active than their Λ_{Fe} enantiomers. Hydroxyl ($\mathbf{L^{3b}}$) or methoxy ($\mathbf{L^{3c}}$) functionality at position X reduces the observed activity *ca* 4-fold compared with the parent compound bearing $\mathbf{L^{3a}}$, whereas the benzyloxy ($\mathbf{L^{3d}}$) and pyrazine ($\mathbf{L^{3e}}$) compounds had similar activity. The same eight compounds as a group showed substantially higher activity against HCT116 $p53^{++}$, with several examples in the nanomolar range. Δ_{Fe}-$\mathbf{L^2}$ compounds are more active than the Λ_{Fe} enantiomers. Enantiomers of $\mathbf{L^{3a}}$ and benzyloxy ($\mathbf{L^{3d}}$) compounds are up to seven times more potent than cisplatin while the others, noticeably the hydroxyl ($\mathbf{L^{3b}}$) are much less so.

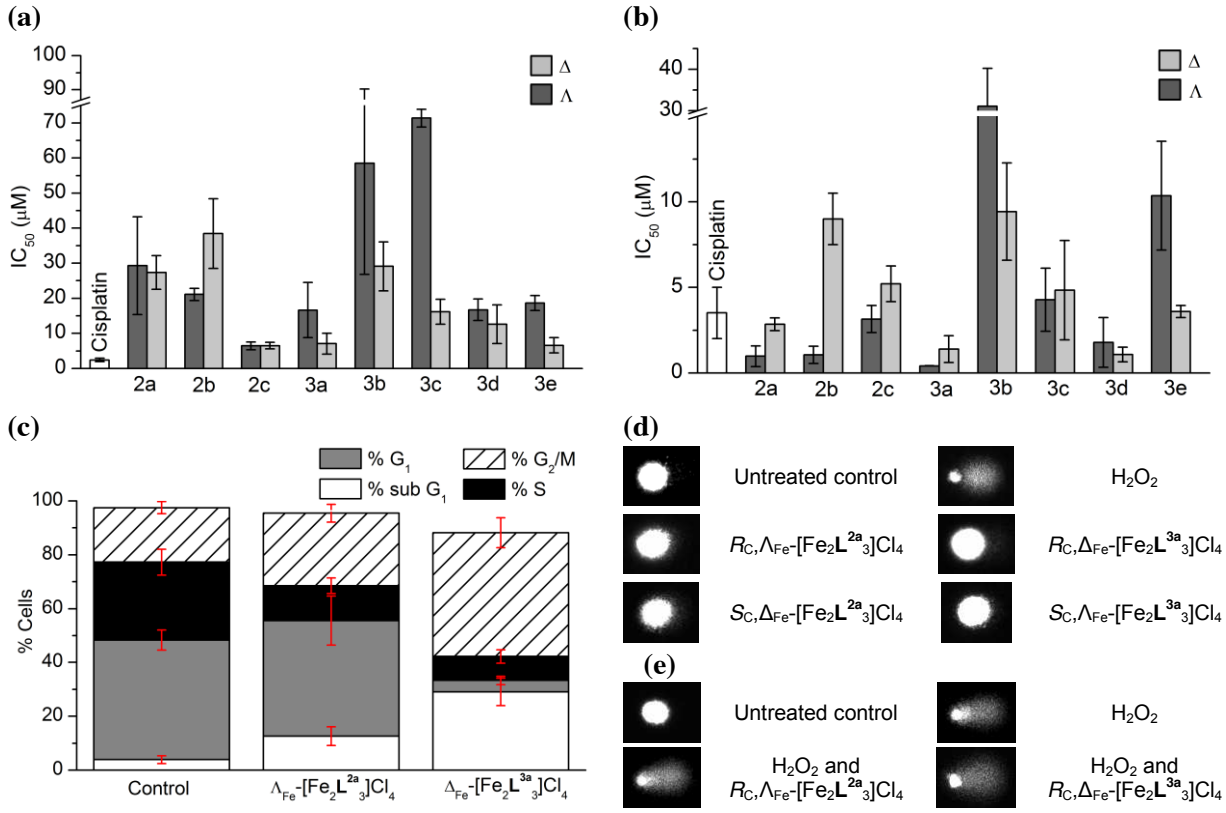

Fig 3 | Exposure of cancer cells to triplex metallohelices. IC_{50} values between 500 nM and 70 μM following 96 h exposures at 37 °C and 5 % CO_2 against (a) human breast adenocarcinoma MDA-MB-468 showing modest toxicity cf. cisplatin and (b) human colon carcinoma HCT116 p53++ showing substantially higher and structure-dependent activity ; (c) Fluorescence-activated cell sorting assay showing the % population in stages of the cell cycle for untreated HCT116 $p53^{++}$ cells and those exposed to R_C,Δ_{Fe},HHT-$[Fe_2\mathbf{L}^{\mathbf{2a}}{}_3]Cl_4$ and R_C,Λ_{Fe},HHT-$[Fe_2\mathbf{L}^{\mathbf{3a}}{}_3]Cl_4$ (10 μM) for 24 h; (d) Comet assay analysis of DNA strand break induction in untreated HCT116 $p53^{++}$ cells and those exposed to hydrogen peroxide, HHT-$[Fe_2\mathbf{L}^{\mathbf{3a}}{}_3]Cl_4$ or HHT-$[Fe_2\mathbf{L}^{\mathbf{2a}}{}_3]Cl_4$ (10 μM) for 24 h; (e) Comet assay analysis of DNA cross link induction in untreated HCT116 $p53^{++}$ cells and those exposed to hydrogen peroxide and HHT-$[Fe_2\mathbf{L}^{\mathbf{3a}}{}_3]Cl_4$ or HHT-$[Fe_2\mathbf{L}^{\mathbf{2a}}{}_3]Cl_4$ (10 μM) for 24 h. Errors shown are the calculated standard deviations from three repeats of each assay.

Clinical anticancer treatments commonly include the use of DNA-binding or modifying drugs such as cisplatin. Such "alkylators" and DNA cleavage agents cause chemically irreversible reactions leading, in the absence of repair, to cell death.[38,39] While the metal ions here are intended to be structure-forming rather than reactive, and since some binding to naked calf thymus (ct-) DNA was detected by DNA melting (ΔT_M +3 - 13 °C), we sought to exclude the possibility of DNA damage. In a single cell gel electrophoresis assay, the absence of a 'comet' tail for HCT116 $p53^{++}$ cells that had been treated with R_C,Λ_{Fe},HHT-$[Fe_2\mathbf{L}^{\mathbf{2a}}{}_3]Cl_4$ or R_C,Δ_{Fe},HHT-$[Fe_2L^{\mathbf{3a}}{}_3]Cl_4$ indicates the absence of breaks (both single and double strand) and alkali labile sites. In a related test, triplexes also failed to retard the formation of comets in cells with deliberately strand-damaged DNA, consistent with the absence of cross linking activity. In addition, these compounds did not significantly alter the production of γ-H2AX – a histone regarded as a universal marker for DNA damage.[40]

The accumulation of cancer cells in particular phases of the cell cycle can point to mode of action.[41] Following incubation with triplex metallohelices10 μM, 24 h) and staining, HCT116 $p53^{++}$ cells were analysed by fluorescence-activated cell sorting (FACS).[41] Compared with control untreated cells, compound R_C,Δ_{Fe},HHT-$[Fe_2\mathbf{L^{3a}}_3]Cl_4$ caused a dramatic increase in the proportion of cells in the G_2/M phase (from *ca* 20 to 46% of cells) and sub G_1 phase (*ca* 4 to 30%) and a corresponding reduction in G_1 phase (*ca* 44 to 4%) and S phase (*ca* 29 to 9%). Cells in the sub G_1 phase are considered apoptotic[42,43] and this data indicates that triplex helicates induce programmed cell death in HCT116 $p53^{++}$ colon carcinoma cells. R_C,Λ_{Fe},HHT-$[Fe_2\mathbf{L^{2a}}_3]Cl_4$ showed a similar but less extreme effect.

Given the high potency and substantial effects on the cancer cell cycle, we were very surprised to discover that enantiomers of the parent triplex compounds showed no signs of toxicity (bactericidal or inhibitory action) towards Methicillin-Resistant *Staphylococcus aureus* (MRSA - USA300) or *Escherichia coli* (TOP10) at up to the highest measured concentration of 128 μg/ml i.e. two orders of magnitude higher than the recorded IC_{50} values against the cancer cell lines.

Discussion

A strategy for the selective formation of anti-parallel 'triplex' metallohelices has been successfully established though molecular modelling, synthetic and structural studies. Ultimately, while absolute configuration at the metal centres was achieved by conventional diastereoselection, the far greater challenge of selectivity for the target asymmetric HHT structure was achieved by maximisation of π-stacking and other secondary interactions between ligands. Specifically, the relatively strong phenyl-bpy π-stacks and in some cases bifurcated C-H…O/N interactions are present only in the triplex architectures. This indicates how other new systems can be designed. These secondary interactions contribute also to chemical stability such that rates of hydrolysis in biologically-relevant media are exceptionally low. In addition, the modular self-assembly has allowed us to produce what we believe to be the largest and most diverse library of metallohelices to date. The potential recognition elements are arranged by the nature of the helix fold, and thereby via selection of molecular sub-component, a number of functional architectures can be made. We believe that this takes us a significant step towards α-helix-peptide-like candidates for biochemical targets and phenotypic screens.

To this end, and as with the peptidic α-helices they are designed to emulate, triplex metallohelices have been shown to display potent, selective and structure-dependent toxicity to certain cancer cell-lines and – remarkably – no measured toxicity to example Gram positive and Gram negative bacteria. This is particularly striking given that our earlier symmetrical *flexicate* compounds inhibit bacterial growth at low concentrations.[32] A subtle biomimetic mechanism rather than broad-

spectrum cytotoxicity is thus indicated, and this is corroborated by the observation of major changes to the cell cycle without detected DNA damage. In future work we will establish whether an extrinsic or intrinsic pathway for apoptosis has been activated: do triplexes interact with membrane proteins or enter the cell and interfere with key internal pathways?

The remarkable selectivity and stability, the unprecedented scope for structural variation, and the potent and selective activity suggest that triplex metallohelices may represent a new area of chemical space for the synthesis of novel pharmaceuticals.

Methods

Full details of computations, synthesis, characterisation and microbiological experiments are given in the Supplementary Information. Outlines of key procedures are detailed below.

Molecular mechanics and DFT calculations

Monometallic structures were first optimised using B3LYP-D3(BJ)[44] functional and the 6-31g(d) basis set, with convergence criteria of 0.0001 a.u. as implemented in the Firefly quantum chemistry package,[45] which is partially based on the GAMESS(US) source code.[46] Bimetallic systems were optimised using ligand field molecular mechanics (LFMM)[47] as implemented in the DommiMOE program,[48] before being annealed at 500 K for 1 ns prior to re-optimisation. Single point energies were determined using the B3LYP-D3(BJ)[44] functional and the def2-TZVP basis set.[45]

Synthesis of water soluble triplex metallohelices

Anhydrous iron(II) chloride (2 eq.) was add to a stirred solution of the either the desired chiral amine (3 eq.) and 5-(2,2'-bipyridin-5-ylmethoxy)picolinaldehyde (3 eq.) or the desired substituted aldehyde (3 eq.) and (*R*)-2-(2,2'-bipyridin-5-ylmethoxy)-1-phenylethanamine (3 eq.) in methanol (20 ml) at ambient temperature to give a purple solution that was then heated to reflux (65°C) for 24 – 48 h. The mixture was allowed to cool to ambient temperature, filtered through a celite plug and the solvents were removed *in vacuo* to give a dark purple solid (>95% yield). Water of crystallisation in these compounds was confirmed by NMR and IR spectroscopy. The hydration number was then determined by thermogravimetric analysis and the relevant mass loss was correlated with microanalytical data. NMR, IR and MS data were consistent with the proposed formulations. CD spectra of enantiomers in water were equal and opposite.

Stability in aqueous media

Visible absorbance spectra for stability studies were recorded using a Carey IE spectrometer. The intensity of the MLCT band (500-600 nm) of a 0.03 mM solution of each compound was measured over time in RPMI cell culture medium at 37°C, and also in 0.2 M hydrochloric acid at 20°C so that comparative $t_{1/2}$ values for hydrolysis could be obtained.

Chemosensitivity (MTT assay)

Cells were incubated in 96-well plates at a cell concentration of 2.0×10^4 cells/ml in RPMI-1640, supplemented with 10% foetal calf serum, sodium pyruvate (1 mM) and l-glutamine (2 mM). Plates were incubated for 24 h at 37°C in an atmosphere of 5% CO_2, prior to drug exposure, then incubated for 96 h. 3-(4,5-Dimethylthiazol-1-yl)-2,5-diphenyltetrazolium bromide (MTT) solution (0.5 mg/ml) was added to each well and incubated for a further 4 h. The IC_{50} values were determined from a plot of percentage cell survival against drug concentration (μM). All assays were conducted in triplicate and the mean IC_{50} ± standard deviation was determined.

γ-H2AX assay

In triplicate, and against untreated control cells, drug-treated HCT116 wild type p53 cells were washed twice in incubation buffer (PBS containing BSA) then re-suspended. Primary rabbit anti-human phosphor Histone H2AX (Ser 139) antibody (1:50 final dilution) was added and incubated at RT for 1 h before treatment with Alexa Fluor conjugated anti-rabbit IgG secondary antibody (1:1000 final dilution) and incubation for 30 min before fluorescence activated cell sorting (FACS).

Cell cycle assay

300 μl PBS containing Propidium Iodide (40 μg/ml) and RNAse A (200μg/ml) was added to drug-treated cells before incubation for 30 min and FACS analysis. The assay was repeated four times with each compound and the mean % cells in each phase ± standard deviation was determined. Red fluorescence was observed at 488nm excitation by flow cytometry and data analysed using WinMDI2.9 and Cylchred software.

Single cell gel electrophoresis (comet) assays

Cells were seeded in complete RPMI-1640 medium and incubated, then treated with drug (10 μM, 24 h), washed, harvested and embedded in agarose. Following horizontal gel electrophoresis (25 min) the slides were stained with SYBR™ Gold solution (Molecular probes Inc.) and viewed with an epifluorescent microscope (Nikon Eclipse E800, Japan). The tail moment was measured on 50 randomly selected cells using Comet assay III software (Perceptive Instruments, UK). Each assay was performed in triplicate.

Antimicrobial Experiments

The standardised macrobroth dilution method[49] in cation-adjusted Mueller-Hinton broth was used. Bacterial growth was monitored over 20 h at 37 °C with an iEMS 96-well plate reader. The lowest concentration to inhibit growth across each repeat is classified as the MIC. Positive (medium and untreated bacteria) and negative (medium only) controls were run with each plate. The antimicrobial properties of our recently reported flexicate systems[32] were reproduced as a positive control, alongside ampicillin.

Acknowledgements

We thank the EPSRC and the University of Warwick for financial support. We thank the National Crystallographic Service for recording the x-ray data (structure code AF20).[50]

Author Contributions

ADF performed the computational work under the direction of DJF; ADF and RAK synthesised and characterised the compounds following early studies by SEH, and developed and conducted stability studies; RAK and QMAA performed the biological work under the direction of RMP; PG developed a synthesis of $[Fe_2(C_{25}H_{20}N_4)_3]Cl_4$ and performed stability studies; GJC solved and refined the X-ray crystal data; DHS conducted the antimicrobial experiments under the direction of DIR; PS conceived and directed the project, interpreted the data and wrote the paper.

Figure Legends & Tables

Figure 1 | Metallohelix architectures.

Figure 2 | Synthesis and characterisation of triplex metallohelices.

Figure 3 | Exposure of cancer cells to triplex metallohelices.

Table 1 | Calculated energies (DFT) of selected isomers for monometallic units and metallohelices.

References

1 Zanetti, M., Gennaro, R. & Romeo, D. Cathelicidins: a novel protein family with a common proregion and a variable C-terminal antimicrobial domain. *FEBS Letters* **374**, 1-5, (1995).

2 Lane, D. P. p53, guardian of the genome. *Nature* **358**, 15-16, (1992).

3 Dürr, U. H. N., Sudheendra, U. S. & Ramamoorthy, A. LL-37, the only human member of the cathelicidin family of antimicrobial peptides. *Biochimica et Biophysica Acta (BBA) - Biomembranes* **1758**, 1408-1425, (2006).

4 Wu, W. K. K. *et al.* Emerging roles of the host defense peptide LL-37 in human cancer and its potential therapeutic applications. *International Journal of Cancer* **127**, 1741-1747, (2010).

5 Baker, S. J. *et al.* Chromosome 17 Deletions and p53 Gene Mutations in Colorectal Carcinomas. *Science* **244**, 217-221, (1989).

6 Takahashi, T. *et al.* p53: A Frequent Target for Genetic Abnormalities in Lung Cancer. *Science* **246**, 491-494, (1989).

7 Walensky, L. D. *et al.* Activation of Apoptosis in Vivo by a Hydrocarbon-Stapled BH3 Helix. *Science* **305**, 1466-1470, (2004).

8 Gavathiotis, E. *et al.* BAX activation is initiated at a novel interaction site. *Nature* **455**, 1076-1081, (2008).

9 Cheng, R. P., Gellman, S. H. & DeGrado, W. F. beta-peptides: From structure to function. *Chemical Reviews* **101**, 3219-3232, (2001).

10 Appella, D. H., Christianson, L. A., Karle, I. L., Powell, D. R. & Gellman, S. H. beta-peptide foldamers: Robust Helix formation in a new family of beta-amino acid oligomers. *Journal of the American Chemical Society* **118**, 13071-13072, (1996).

11 Johnson, L. M. & Gellman, S. H. in *Methods in Protein Design* Vol. 523 *Methods in Enzymology* (ed A. E. Keating) 407-429 (2013).

12 Davis, J. M., Tsou, L. K. & Hamilton, A. D. Synthetic non-peptide mimetics of alpha-helices. *Chem. Soc. Rev.* **36**, 326-334, (2007).

13 Azzarito, V., Long, K., Murphy, N. S. & Wilson, A. J. Inhibition of [alpha]-helix-mediated protein-protein interactions using designed molecules. *Nat Chem* **5**, 161-173, (2013).

14 Lehn, J. M. *et al.* Spontaneous assembly of double-stranded helicates from oligobipyridine ligands and copper(I) cations: structure of an inorganic double helix. *Proc. Natl. Acad. Sci. U.S.A.* **84**, 2565-2569, (1987).

15 Albrecht, M. & Fröhlich, R. Controlling the Orientation of Sequential Ligands in the Self-Assembly of Binuclear Coordination Compounds. *J. Am. Chem. Soc.* **119**, 1656-1661, (1997).

16 Torelli, S., Delahaye, S., Hauser, A., Bernardinelli, G. & Piguet, C. Ruthenium(II) as a novel labile partner in thermodynamic self-assembly of heterobimetallic d-f triple-stranded helicates. *Chem. Eur. J.* **10**, 3503-3516, (2004).

17 Hahn, F. E., Schulze Isfort, C. & Pape, T. A dinuclear, triple-stranded helicate with a diamide-bridged catechol/benzenedithiol ligand. *Angewandte Chemie* **43**, 4807-4810, (2004).

18 Rice, C. R., Baylies, C. J., Jeffery, J. C., Paul, R. L. & Ward, M. D. Mononuclear Cu(II) and triple helical dinuclear Co(II) complexes of a new potentially tetradentate ligand containing inequivalent bidentate units. *Inorganica Chimica Acta* **324**, 331-335, (2001).

19 Hannon, M. J., Bunce, S., Clarke, A. J. & Alcock, N. W. Spacer Control of Directionality in Supramolecular Helicates Using an Inexpensive Approach. *Angewandte Chemie International Edition* **38**, 1277-1278, (1999).

20 Constable, E. C., Heirtzler, F. R., Neuburger, M. & Zehnder, M. Directional ligands in helicate selfassembly. *Supramol. Chem.* **5**, 197-200, (1995).

21 Albrecht, M., Napp, M., Schneider, M., Weis, P. & Frohlich, R. Kinetic thermodynamic control of the self-assembly of isomeric double-stranded dinuclear titanium() complexes from a phenylalanine-bridged dicatechol ligand. *Chemical Communications*, 409-410, (2001).

22 Schulze Isfort, C., Kreickmann, T., Pape, T., Frohlich, R. & Hahn, F. E. Helical complexes containing diamide-bridged benzene-o-dithiolato/catecholato ligands. *Chemistry* **13**, 2344-2357, (2007).
23 Howson, S. E. & Scott, P. Approaches to the synthesis of optically pure helicates. *Dalton Trans.* **40**, 10268-10277, (2011).
24 Kerckhoffs, J. M. C. A. *et al.* Enantiomeric resolution of supramolecular helicates with different surface topographies. *Dalton Trans.*, 734-742, (2007).
25 Hotze, A. C. G. *et al.* Supramolecular iron cylinder with unprecedented DNA binding is a potent cytostatic and apoptotic agent without exhibiting genotoxicity. *Chem. Biol.* **15**, 1258-1267, (2008).
26 Cardo, L., Sadovnikova, V., Phongtongpasuk, S., Hodges, N. J. & Hannon, M. J. Arginine conjugates of metallo-supramolecular cylinders prescribe helicity and enhance DNA junction binding and cellular activity. *Chem. Commun.* **47**, 6575-6577, (2011).
27 Yu, H. *et al.* Metallosupramolecular complex targeting an a/b discordant stretch of amyloid b peptide. *Chem. Sci.* **3**, 3145-3153, (2012).
28 Howson, S. E. *et al.* Origins of stereoselectivity in optically pure phenylethaniminopyridine *tris*-chelates $M(NN')_3^{n+}$ (M = Mn, Fe, Co, Ni and Zn). *Dalton Trans.* **40**, 10416-10433, (2011).
29 Howson, S. E. *et al.* Self-assembling optically pure Fe(A-B)3 chelates. *Chem. Commun.* **0**, 1727-1729, (2009).
30 Howson, S. E. *et al.* Jahn-Teller effects on p-stacking and stereoselectivity in the phenylethaniminopyridine tris-chelates $Cu(NN')_3^{2+}$. *Dalton Trans.* **41**, 4477-4483, (2012).
31 Howson, S. E. *et al.* Optically pure heterobimetallic helicates from self-assembly and click strategies. *Dalton Transactions* **42**, 14967-14981, (2013).
32 Howson, S. E. *et al.* Optically pure, water-stable metallo-helical 'flexicate' assemblies with antibiotic activity. *Nat. Chem.* **4**, 31-36, (2012).
33 Brabec, V. *et al.* Metallohelices with activity against cisplatin-resistant cancer cells; does the mechanism involve DNA binding? *Chemical Science*, (2013).
34 Hunter, C. A. & Sanders, J. K. M. The nature of .pi.-.pi. interactions. *J. Am. Chem. Soc.* **112**, 5525-5534, (1990).
35 Grimme, S. Do Special Noncovalent π–π Stacking Interactions Really Exist? *Angewandte Chemie International Edition* **47**, 3430-3434, (2008).
36 Hannon, M., J. , Painting, C., L. , Jackson, A., Hamblin, J. & Errington, W. An inexpensive approach to supramolecular architecture. *Chem. Commun.*, 1807-1808, (1997).
37 Ren, S. X. *et al.* FK-16 Derived from the Anticancer Peptide LL-37 Induces Caspase-Independent Apoptosis and Autophagic Cell Death in Colon Cancer Cells. *PLoS ONE* **8**, e63641, (2013).
38 Fu, D., Calvo, J. A. & Samson, L. D. Balancing repair and tolerance of DNA damage caused by alkylating agents. *Nat. Rev. Cancer* **12**, 104-120, (2012).
39 Siddik, Z. H. Cisplatin: mode of cytotoxic action and molecular basis of resistance. *Oncogene* **22**, 7265-7279, (2003).
40 Bonner, W. M. *et al.* [gamma]H2AX and cancer. *Nat Rev Cancer* **8**, 957-967, (2008).
41 Krishan, A. Rapid flow cytofluorometric analysis of mammalian cell cycle by propidium iodide staining. *The Journal of Cell Biology* **66**, 188-193, (1975).
42 Nicoletti, I., Migliorati, G., Pagliacci, M. C., Grignani, F. & Riccardi, C. A rapid and simple method for measuring thymocyte apoptosis by propidium iodide staining and flow cytometry. *Journal of Immunological Methods* **139**, 271-279, (1991).
43 Kajstura, M., Halicka, H. D., Pryjma, J. & Darzynkiewicz, Z. Discontinuous fragmentation of nuclear DNA during apoptosis revealed by discrete "sub-G1" peaks on DNA content histograms. *Cytometry Part A* **71A**, 125-131, (2007).
44 Grimme, S., Ehrlich, S. & Goerigk, L. Effect of the damping function in dispersion corrected density functional theory. *Journal of Computational Chemistry* **32**, 1456-1465, (2011).

45 Granovsky, A. A. *Firefly version 7.1.G,* http://classic.chem.msu.su/gran/firefly/index.html.
46 Schmidt, M. W. *et al.* General atomic and molecular electronic structure system. *Journal of Computational Chemistry* **14**, 1347-1363, (1993).
47 Deeth, R. J., Anastasi, A., Diedrich, C. & Randell, K. Molecular modelling for transition metal complexes: Dealing with d-electron effects. *Coord. Chem. Rev.* **253**, 795-816, (2009).
48 Deeth, R. J., Fey, N. & Williams–Hubbard, B. DommiMOE: An implementation of ligand field molecular mechanics in the molecular operating environment. *J. Comput. Chem.* **26**, 123-130, (2005).
49 Andrews, J. M. Determination of minimum inhibitory concentrations. *Journal of Antimicrobial Chemotherapy* **48**, 5-16, (2001).
50 Coles, S. J. & Gale, P. A. Changing and challenging times for service crystallography. *Chemical Science* **3**, 683-689, (2012).